BJC British Journal of Cancer

www.nature.com/bjc

ARTICLE

Molecular Diagnostics

Radiomics predicts risk of cachexia in advanced NSCLC patients treated with immune checkpoint inhibitors

Wei Mu[1], Evangelia Katsoulakis[2], Christopher J. Whelan[1], Kenneth L. Gage[3], Matthew B. Schabath[4,5] and Robert J. Gillies[1]

BACKGROUND: Approximately 50% of cancer patients eventually develop a syndrome of prolonged weight loss (cachexia), which may contribute to primary resistance to immune checkpoint inhibitors (ICI). This study utilised radiomics analysis of ^{18}F-FDG-PET/CT images to predict risk of cachexia that can be subsequently associated with clinical outcomes among advanced non-small cell lung cancer (NSCLC) patients treated with ICI.

METHODS: Baseline (pre-therapy) PET/CT images and clinical data were retrospectively curated from 210 ICI-treated NSCLC patients from two institutions. A radiomics signature was developed to predict the cachexia with PET/CT images, which was further used to predict durable clinical benefit (DCB), progression-free survival (PFS) and overall survival (OS) following ICI.

RESULTS: The radiomics signature predicted risk of cachexia with areas under receiver operating characteristics curves (AUCs) ≥ 0.74 in the training, test, and external test cohorts. Further, the radiomics signature could identify patients with DCB from ICI with AUCs≥0.66 in these three cohorts. PFS and OS were significantly shorter among patients with higher radiomics-based cachexia probability in all three cohorts, especially among those potentially immunotherapy sensitive patients with PD-L1-positive status ($p < 0.05$).

CONCLUSIONS: PET/CT radiomics analysis has the potential to predict the probability of developing cachexia before the start of ICI, triggering aggressive monitoring to improve potential to achieve more clinical benefit.

British Journal of Cancer (2021) 125:229–239; https://doi.org/10.1038/s41416-021-01375-0

BACKGROUND

Cachexia, a syndrome that induces progressive functional impairment,[1] occurs in about 50% of all cancer patients[2] and accounts for 20% of cancer-related deaths.[3] Cachexia is defined as more than 5% weight loss over 6 months, or more than 2% weight loss if body mass index (BMI) is less than 20 kg/m^2 in absence of simple starvation.[4] Compared to breast cancer, thyroid cancer and haematological malignancies, the development of cachexia is higher in patients with lung cancer.[5,6] Notably, chronic obstructive pulmonary disease (COPD), is a very high risk factor for development of cachexia,[7,8] although the mechanisms triggering this are unknown. Cancer cachexia not only increases patients' mortality, but also impairs the response to first and second line chemo- and radio-therapies.[5] Additionally, cachexia promotes primary resistance to immune checkpoint inhibitors (ICIs), which otherwise significantly improves durable clinical benefit (DCB), progression-free survival (PFS) and overall survival (OS) in non-small cell lung cancer (NSCLC) patients.[9,10] This resistance is hypothesised to be caused by suboptimal drug exposure as anorexia/cachexia-related metabolic wasting may accelerate antibody blood clearance.[11,12] Therefore, early identification of patients likely to develop cachexia could be used to initiate interventions as early as possible to attenuate cachexia progression.[13] If successful, these interventions would improve prognosis of response to ICIs.[5]

To identify patients at risk of developing cachexia at early stage, prior studies have attempted to define criteria for pre-cachexia, a stage when early clinical and metabolic signs such as anorexia and inflammation were present, but substantial weight loss was not.[4] Predictive criteria that have been investigated have included: weight loss, body mass index (BMI),[14] anorexia, systemic inflammation,[15] biochemistry, food intake, activities and functional status.[16] However, these studies were analysed based on overall survival, and could not be used for predicting cachexia directly.

Cancer-associated cachexia is caused by tumour- and host-derived factors that lead to inflammation, and systemic metabolic modifications, including excess catabolism, increased energy expenditure and progressive loss of muscle.[11,17,18] Metabolic alterations associated with malignant disease may alter lymphocyte function by limiting the availability of key nutrients.[19] Besides cancer-induced cachexia, some chemotherapies also induce cachexia-like loss of muscle and adipose tissue. Fearon et al. suggested that therapy-induced weight loss may be considered an "integral part" of the syndrome.[1] This perspective is borne out by later studies that have shown that cancer-induced and therapy-induced cachexia share some signalling pathways.[20] These include

[1]Department of Cancer Physiology, H. Lee Moffitt Cancer Center and Research Institute, Tampa, FL, USA; [2]James A. Haley Veterans' Hospital, Tampa, FL, USA; [3]Department of Radiology, H. Lee Moffitt Cancer Center and Research Institute, Tampa, FL, USA; [4]Department of Cancer Epidemiology, H. Lee Moffitt Cancer Center and Research Institute, Tampa, FL, USA and [5]Department of Thoracic Oncology, H. Lee Moffitt Cancer Center and Research Institute, Tampa, FL, USA
Correspondence: Matthew B. Schabath (matthew.schabath@moffitt.org) or Robert J. Gillies (Robert.Gillies@moffitt.org)
These authors jointly supervised this work: Matthew B. Schabath, Robert J. Gillies.

Received: 3 December 2020 Revised: 10 March 2021 Accepted: 17 March 2021
Published online: 7 April 2021

pathways involved in muscle wasting[21,22] and some that may interfere with muscle anabolism.[21,23] Therefore, we do not attribute the manifestation of cachexia to one cause or the other, hereafter referring to both cancer-induced and therapy-induced cachexia simply as cachexia.

As a metabolic imaging technique, ^{18}F-FDG PET/CT is sensitive in reflecting metabolic changes. ^{18}F-FDG uptake assessed by PET/CT not only reports on the metabolic status of the tumour cells, but it can also be associated inflammatory cellular and molecular alterations,[24] and to reflect not only the number of lymphocytes, but also the activation state of the lymphocytes themselves.[25] Further, the recently developed "radiomics" analyses, which converts medical images into high-dimensional mineable data,[26] can predict therapy response to ICI,[27–29] as well as successfully predict tumour gene mutations[30] and protein expression[31] status. However, the association between PET/CT-based radiomics and cachexia has not been well investigated. Therefore, we hypothesise that radiomics analysis of the primary tumour from pre-treatment PET/CT images can reveal subtle effects on tumour cell metabolism and predict the probability of developing cachexia.

In this study, we develop and validate a radiomics model to predict subsequent development of cachexia during the course of ICI in NSCLC patients, and we demonstrate that the generated radiomics signature has prognostic value.

METHODS

Study population

Retrospective patient cohorts were identified from two institutions: H. Lee Moffitt Cancer Center & Research Institute (HLM) and the James A. Haley Veterans' Hospital (VA), both in Tampa, Florida. Inclusion criteria included patients with histologically confirmed advanced stage (IIIB and IV) NSCLC who were treated with anti-PD-1 or anti-PD-L1 immune checkpoint blockade between June 2011 and August 2019. The detailed exclusion criteria are provided in Supplementary Fig S1 and include: (a) PET/CT images not available before the start of immunotherapy; (b) ≥3 months between the PET/CT acquisition and the start of immunotherapy; (c) other treatments that were performed between imaging acquisition and start of treatment; (d) follow-up time of <6 months after the start of treatment; (e) no weight record 6 months after the start of the immunotherapy. Thus, 175 patients from HLM were randomly split 70:30 into training ($N = 123$) and test cohorts ($N = 52$) with the condition that these two cohorts had the same cachexia incidence rate. An additional 35 external test patients from the VA were used to further test the radiomics signature to predict cachexia, and to investigate the association of the radiomics signature on clinical outcomes.

Clinical characteristics including age at diagnosis, sex, body mass index (BMI), smoking status, history of COPD (chronic obstructive pulmonary disease), Eastern Clinical Oncology Group (ECOG) performance status (PS), distant metastasis (M), PD-L1 status, weight at diagnosis and 6 months later after ICI treatment were obtained from the medical records. BMI was categorised according to: below 20.0 kg/m^2, underweight; 20.0–24.9 kg/m^2, normal weight; 25.0–29.9 kg/m^2, overweight; and above 30.0 kg/m^2, obese.[32] Development of cachexia after the initiation of ICI was defined as patients with more than 5% weight loss over past 6 months, or more than 2% weight loss with body mass index (BMI) less than 20 kg/m^2. The level of PD-L1 expression was presented as a tumour proportion score (TPS), which is the percentage of viable tumour cells showing membrane PD-L1 staining relative to all viable tumour cells, and PD-L1 positivity was defined as ≥1% of TPS. Progression-free survival (PFS) and overall survival (OS) were the endpoints of the study and were assessed from start date of immunotherapy to the date of an event or last follow-up. For PFS, an event was progression defined according to Response Evaluation Criteria in Solid Tumors (RECIST1.1), and for OS, an event was death.

This study was approved by the Institutional Review Boards at University of South Florida (USF) and the James A. Haley Veterans Hospital and was conducted in accordance with ethical standards of the 1964 Helsinki Declaration and its later amendments.

PET/CT image analysis

The details of PET/CT imaging analysis are presented in Supplementary section 1 and the pipeline of this study is provided in Fig. 1. Briefly, all PET images were converted into SUV units by normalising the activity concentration to the dosage of ^{18}F-FDG injected and the patient body weight after decay correction. Muscles were identified in two to four adjacent axial images within the CT series at the third lumbar vertebra slice by slice, including rectus abdominus, abdominal (lateral and oblique), psoas, and paraspinal (quadratus lumborum, erector spinae) by a 5-year experienced orthopaedist (Y. W.) who was blinded to the clinical outcomes using ITK-SNAP software. These images were refined with a Hounsfield unit (HU) range of −29 to 150 averaged for each patient. The total muscle cross-sectional area (cm^2) was normalised for height in meters squared (m^2) and reported as lumbar Skeletal Muscle Index (SMI) in cm^2/m^2.[32] The masks of the lumbar skeletal muscle from CT images were applied to the PET images, and basic metabolic features (SUVmax, SUVmean, SUV Variance, SUVpeak and total lesion glycolysis (TLG = MTV × SUVmean) were calculated.

The primary lung tumours of PET and CT images were semi-automatically segmented with an improved level-set method based on the gradient fields and refined by a radiologist with 16 years of experience (J. Q) who was also blinded to the outcome[29,33] (Supplementary Fig S2), and 30 randomly selected nodules in the training cohort were segmented twice. After spatial registration using a rigid transformation by maximising the Dice Similarity Coefficients on the condition that the maximal axial cross sections of the tumour nodules were aligned, fusion images were generated from the fused PET and CT images on a voxel-wise basis. Additionally, on each tumour-restricted PET image, Otsu thresholding[34] was performed to automatically maximise inter-class variance. Using the obtained threshold, the corresponding tumour of PET images was divided into high and low metabolic (SUV) regions, representing distinct habitats. The masks of these two habitats were then mapped to the co-registered CT images, and two CT sub-regions were subsequently obtained. Therefore, four sub-regions regions of PET and CT images including PEThigh, PETlow, CThigh and CTlow were included. Consequently, 1053 quantitative features (364 whole-tumour PET features, 364 whole-tumour CT features, 65 fusion features and 260 habitat imaging-based features) were extracted. The process of radiomics feature extraction was performed in MATLAB 2020a (MathWorks) in compliance with the Image-Biomarker-Standardization-Initiative (IBSI) guidelines.[35]Details are provided in Supplementary Section 2.

Development of the radiomics signature

To reduce the dimension of the radiomics features, a four-step feature selection procedure was performed to obtain the key radiomic features to predict cachexia. First, the inter-rater agreement of the radiomics features were calculated by intraclass correlation coefficient (ICC) between segmentations, and only the features with ICC larger than 0.8 were retained. Then, a two-sample *t*-test was used to pre-select the radiomics features that were significantly ($P < 0.05$) different between the cachectic and non-cachectic patients. Next, to reduce redundancy, the significantly different features were grouped according to the absolute value Pearson correlation coefficient of 0.9, and only the single feature with the largest classification ability, based on area under

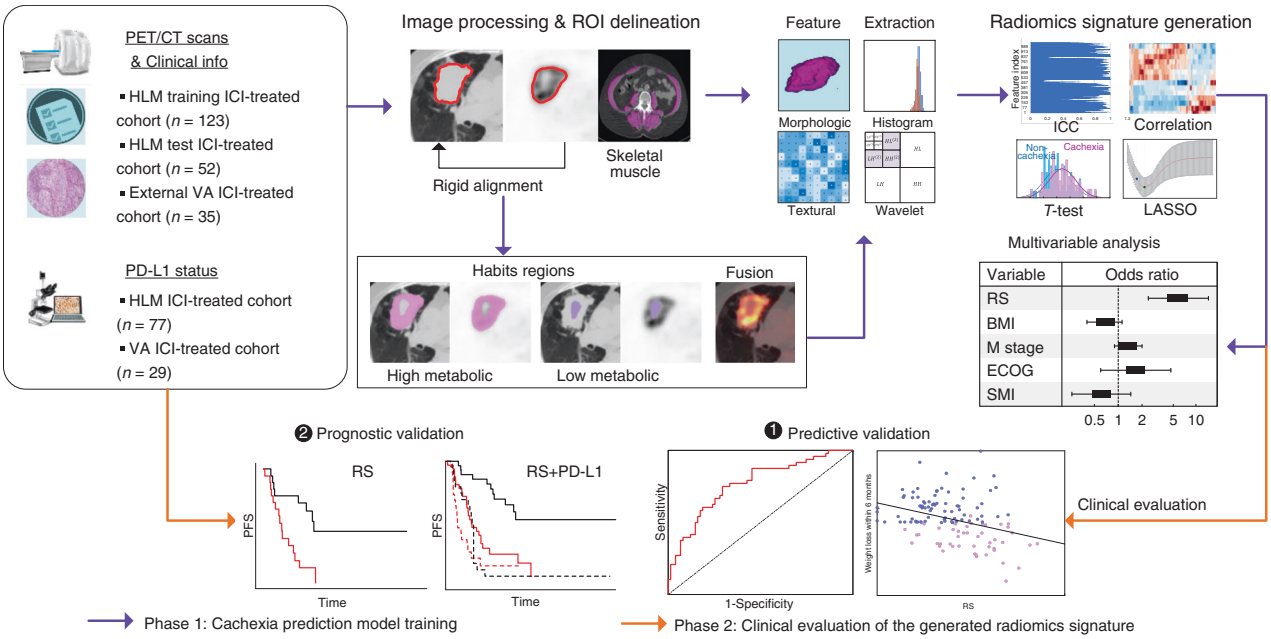

Fig. 1 Study design, which contains two main phases. First, the primary tumour and the skeleton muscle were delineated semi-automatically and the habitats were automatically generated. Then, four categories of image features were calculated, including morphologic, histogram, textural and wavelet features. Next, after feature selection, the radiomics signature (RS) was obtained. For the second phase, this signature was clinically evaluated through predictive validation and prognostic validation.

the receiver operating characteristics curve (AUC), in each group were selected to be representative (the "Avatar") for that group. Finally, a Least Absolute Shrinkage and Selection Operators procedure (LASSO)-logistic regression analysis was used to select the most useful predictive features with non-zero coefficients, and generate the radiomics signature (RS) through a linear combination weighted by the corresponding coefficients.[36] The penalty parameter (λ) in LASSO was selected using 10-fold cross validation by minimum mean cross-validated error. To assess the quality of this radiomics study, the radiomic quality score (RQS) was calculated according to Lambin et al.[37]

Statistical analysis

The Wilcoxon signed-rank test and Fisher's exact test were used to test the differences for continuous variables and categorical variables, respectively. Pearson correlation coefficient was used to test for correlations between continuous variables. The cut-offs of RS and SMI used for the classification of high risk of cachexia were determined by maximising Youden's index based on the training cohort. Univariable and multivariable logistical regression models (backward step-down selection with Akaike information criterion as the stopping rule),[38] which were presented as radiomics nomograms, were used to assess the predictive ability of RS, SMI, clinical common used metrics including SUVmax, MTV (metabolic tumour volume) and volume (from CT images), and other clinical variables (categorised BMI, sex, age, smoke status, COPD, ECOG, distant metastasis and histology). The area under the receiver operating characteristics curve (AUC), accuracy, sensitivity, specificity and the 95% confidence interval (CI) by the Delong method[39] were used to assess the ability of different models in discriminating between cachectic and non-cachectic patients. Z test was applied to compare the differences between different models. To demonstrate the significantly incremental value of different models, total net reclassification improvement (NRI) was calculated. For PFS and OS comparison, Kaplan–Meier analysis and log-rank test were used. *P*-value less than 0.05 was regarded as significant, and statistical analyses were conducted with R (version 3.5.1) and MATLAB (R2020a).

RESULTS

Clinical characteristics

The clinical characteristics of the patients used to train and test the predictor for cachexia are presented in Table 1. Among these 175 patients (96 males, 79 females), the mean age was 66 ± 12 (±standard deviation, SD) years with a median PFS and OS of 8.40 and 27.6 months, respectively. Of these, 69 patients experienced more than 5% weight loss (weight loss: 10.28 ± SD 4.63%) during the first six months of immunotherapy and were regarded as cachectic. All 35 of the external VA patients (Supplementary Table S1) are male, with the mean age of 71.40 ± SD 7.19 years. Ten patients had stage IIIB disease, while the remaining 25 patients were stage IV. The median PFS and OS were 8.13 months and 13.10 months, respectively. Of the 29 patients who had their weight recorded 6 months after the start of the immunotherapy, 14 of them suffered from cachexia with an accompanying weight loss of 8.90 ± SD 3.04%.

Development of the radiomics signature

Within 949 features with ICC larger than 0.8, thirty features were found to be significantly different between the cachexic and non-cachexic patients in the training set. After eliminating redundancy, twenty-seven non-redundant stable features were left and entered into the LASSO analysis. Of these, nine features were selected out of training to construct the radiomics signature, and these were incorporated into the calculation formula as $RS = 0.69 \times CT_{ZSN} - 0.64 \times CT_{Energy} - 0.30 \times CT_{max} + 0.018 \times CThigh_{mean} - 0.70 \times PET_{LD} - 0.15 \times PET_{SRHGE} - 0.30 \times PEThigh_{DD} + 0.35 \times PETlow_{LZLGE} + 0.12 \times FUSE_{MHS} + 0.51$ (Details shown Supplementary section 4). Representative images and radiomics signatures (RS) of two patients from baseline PET/CT scan are shown in Fig. 2a, b.

Diagnostic performance of the radiomics signature

The RS was significantly different between cachexic and non-cachexic patients in the training cohort ($p < 0.001$), which was validated in the test cohort ($p = 0.003$) and external test cohort ($p = 0.040$). Although the RS was obtained based on the binarised

Table 1. Demographic and clinical characteristics of patients.

Characteristic	Training cohort		P^a	Test cohort		P^a	P^b
	Cachexia ($N = 48$)	No-Cachexia ($N = 75$)		Cachexia ($N = 21$)	No-Cachexia ($N = 31$)		
Age (y)			0.21			0.33	0.62
Mean ± SD	64.40 ± 11.31	67.35 ± 9.71		62.33 ± 17.04	66.06 ± 15.15		
Sex, NO. (%)			0.85			1.00	0.41
Male	28 (58.33)	42 (56)		10 (47.62)	16 (51.61)		
Female	20 (41.67)	33 (44)		11 (52.38)	15 (48.39)		
BMI (kg/m2)			0.016[c]			0.30	0.62
Mean ± SD	25.1 ± 5.55	26.97 ± 4.43		25.53 ± 3.47	26.41 ± 5.89		
BMI category (kg/m^2)			0.018[c]			0.066	0.81
<20.0	6 (12.5)	3 (4)		2 (9.52)	0 (0)		
20.0–24.9	21 (43.75)	25 (33.33)		7 (33.33)	14 (45.16)		
25.0–29.9	15 (31.25)	29 (38.67)		10 (47.62)	10 (32.26)		
≥30	6 (12.5)	18 (24)		2 (9.52)	7 (22.58)		
Skeletal muscle index (SMI) (cm^2/m^2)			0.46			0.17	0.50
Mean ± SD	41.52 ± 14.61	42.57 ± 13.35		37.65 ± 11.98	44.74 ± 16.79		
ECOG PS			0.050[c]			0.18	0.83
0	6 (12.5)	23 (30.67)		2 (9.52)	8 (25.81)		
1	40 (83.33)	51 (68)		18 (85.71)	23 (74.19)		
≥2	2 (4.17)	1 (1.33)		1 (4.76)	0 (0)		
Distant metastasis			0.017[c]			0.64	0.45
M0	9 (18.75)	25 (33.33)		4 (19.05)	9 (29.03)		
M1a	6 (12.5)	18 (24)		3 (14.29)	7 (22.58)		
M1b	21 (43.75)	20 (26.67)		11 (52.38)	12 (38.71)		
M1c	12 (25)	12 (16)		3 (14.29)	3 (9.68)		
Histology, NO. (%)			0.077			0.58	0.09
Adenocarcinoma	27 (56.25)	55 (73.33)		12 (57.14)	15 (48.39)		
Squamous cell carcinoma	21 (43.75)	20 (26.67)		9 (42.86)	16 (51.61)		
Weight change within 6 months (%)			<.001[c]			<.001[c]	0.96
Mean ± SD	−10.54 ± 4.65	0.86 ± 5.21		−9.69 ± 4.63	0.5 ± 3.98		
Smoke, NO. (%)			0.84			0.87	0.16
Non-smoker	18 (37.5)	31 (41.33)		5 (23.81)	9 (29.03)		
Former smoker	28 (58.33)	42 (56)		14 (66.67)	20 (64.52)		
Current smoker	2 (4.17)	2 (2.67)		2 (9.52)	2 (6.45)		
COPD			0.14			0.72	0.66
NO. (%)	11 (22.92)	9 (12)		3 (14.29)	7 (22.58)		
PD-L1 status			1.00			0.62	1.00
Positive	11 (22.92)	18 (24.00)		7 (33.33)	2 (6.45)		
Negative	11 (22.92)	17 (22.67)		12 (57.14)	4 (12.90)		
Unknown	26 (54.17)	40 (53.33)		2 (9.52)	25 (80.65)		
Best response			0.050[c]			<0.001[c]	0.67
PR/CR/SD	13 (27.08)	9 (12)		10 (47.62)	1 (3.23)		
PD	35 (72.92)	66 (88)		11 (52.38)	30 (96.77)		
Progression-free survival			0.001[c]			0.005[c]	0.84
Median (IQR)	5.37 (2.60–13.77)	11.93 (7.43–NR)		3 (1.77–9.63)	16 (6.17–50.20)		
Overall survival			0.011[c]			0.009[c]	0.30
Mean(95%CI)	30.99 (5.18–20.84)	38.75 (31.12–46.37)		24.19 (11.90–36.47)	38.72 (28.03-49.40)		
RS			<.001[c]			.003[c]	0.77
Median (IQR)	0.51 (0.40, 0.62)	0.31 (0.22,0.43)		0.49 (0.39,0.60)	0.32 (0.22,0.43)		

Data are patient numbers, with percentages in parentheses. IQR is short for interquartile range; The demographic and clinical characteristics of external VA patients were provided in Supplementary Table S1.
SD standard deviation.
[a]*P*-value is derived between Cachexia and non-Cachexia.
[b]*P* is derived training and test cohorts.
[c]means *P*-value < .05.

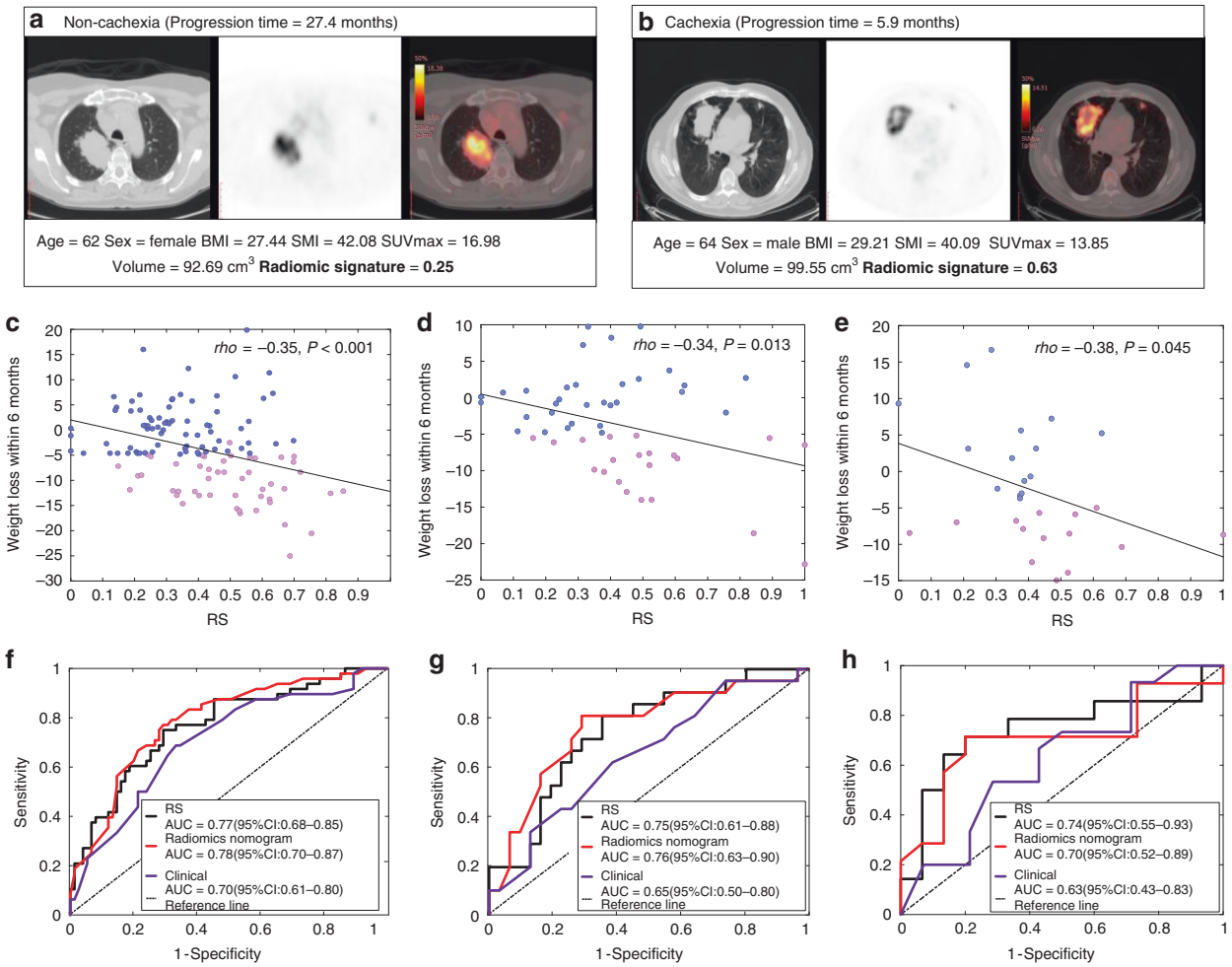

Fig. 2 Radiomics signatures of NSCLC patients and their diagnostic performance in various cohorts. a, b The CT, PET and fusion images for a patient with NSCLC, together with the corresponding clinical variables and radiomics signatures. **c–e** The Pearson correlation between RS and the weight loss within 6 months since the start of the immunotherapy in the training, test and external test cohorts, respectively. *P*-value indicates two-sided Pearson correlation test. **f–h** The ROC curves of RS, radiomics nomogram and clinical models in the training, test and external test cohorts, respectively.

cachexia vs. non-cachexia, the RS was also found to be weakly but significantly correlated with the actual weight change within 6 months since the start of the immunotherapy in both training (Pearson rho = −0.35, $p < 0.001$) and test cohorts (Pearson rho = −0.34, $p = 0.013$) as shown in Fig. 2c, d, indicating that a larger RS corresponds to a larger weight loss. This RS yielded an AUC of 0.77 (95% CI: 0.70–0.84) and 0.75 (95% CI: 0.64–0.85) in the training and test cohorts, respectively, and an accuracy of 72.36% (95% CI: 64.23–80.49) and 71.15% (95% CI: 59.62–82.69) in the training and test cohorts, respectively. Detailed information of radiomics signature performance is shown in Table 2, and the corresponding ROC curves are shown in Fig. 2f, g. Additionally, this signature was also found to be weakly but significantly correlated with the actual weight change within 6 months since the start of the immunotherapy (Pearson rho = −0.38, $p = 0.045$), and had a good performance in the external VA cohort with an AUC of 0.74 (95% CI: 0.55–0.93), accuracy of 72.41% (95% CI: 55.17–86.21%), sensitivity of 71.43% (95% CI:42.86–92.86%) and specificity of 73.33% (95% CI:46.67–93.33%) (Fig. 2e, h).

Although quantitative index of skeletal muscle mass (SMI) has been significantly associated with cachexia in other studies,[32] it was not significant in our study, achieving an AUC of 0.54 (95% CI: 0.43–0.65, $p = 0.46$) and 0.61 (95% CI: 0.46–0.77, $p = 0.17$) in the training and test cohorts, respectively. Through multivariable logistical regression analysis, SMI was also not identified as independently significant in the training cohort ($p = 0.19$), although it was significant in the test cohort ($p = 0.047$). The combination of RS and SMI did not improve the prediction performance compared to the RS alone with AUCs of 0.76 (95% CI:0.67–0.84, $p = 0.77$, Delong test) and 0.74 (95% CI:0.61–0.88, $p = 0.99$, Delong test) in both the training and test cohorts, respectively. A secondary stratified analysis was performed that only analysed the patients without history of cachexia ($n = 57$). For these patients, the SMI was found to be predictive, with an AUC of 0.82 (98% CI: 0.68–0.95, $p = 0.001$), which is similar to the AUC of 0.76 (95% CI:0.60–0.92, $p = 0.009$) for RS in this same cohort ($p = 0.57$, Delong test). The AUC for the combination of RS and SMI was not significantly higher compared to SMI or RS alone ($p = 0.55$, $p = 0.15$, respectively).

Clinical prediction model and decision curve analyses

Univariable logistic regression analysis of the clinical variables showed that categorised BMI, ECOG PS and distant metastasis were all identified as strong predictors for cachexia with $p = 0.018$, $p = 0.017$ and $p = 0.015$, respectively (Supplementary Table S2). None of the basic metabolic features of the skeletal muscle was significantly different between cachectic and non-cachectic patients (Supplementary Table S3). A clinical prediction model was thus trained by incorporating these three clinical variables using multivariable logistic regression analysis, and this achieved

Table 2. Performance of different models in cachexia prediction.

	AUC (95% CI)	ACC (95% CI)	SEN (95% CI)	SPEC (95% CI)	PPV (95% CI)	NPV (95% CI)	AIC
Radiomics signature							
Training	0.77 (0.68–0.85)	72.36 (64.23–80.49)	75.00 (62.5–87.50)	70.67 (60.00–81.33)	62.07 (52.86–71.84)	81.54 (73.85–89.60)	140.4
Test	0.75 (0.60–0.86)	71.15 (59.62–82.69)	80.95 (61.9–95.24)	64.52 (48.39–80.65)	60.71 (48.57–74.07)	83.33 (79.37–95.91)	65.29
External	0.74 (0.55–0.93)	72.41 (55.17–89.66)	71.43 (50–92.86)	73.33 (53.33–93.33)	71.43 (54.44–92.31)	73.33 (57.89–92.86)	40.55
Radiomics Nomogram							
Training	0.78 (0.69–0.86)	73.17 (64.23–80.49)	77.08 (64.58–87.5)	70.67 (60.00–80.63)	62.71 (54.03–72.31)	82.81 (74.64–90.84)	142.9
Test	0.76 (0.61–0.89)	75.00 (61.54–86.54)	80.95 (61.9–95.24)	70.97 (54.84–87.1)	65.38 (52.00–80.00)	84.62 (72.41–96.00)	62.78
External	0.70 (0.52–0.89)	75.86 (62.07–87.66)	71.43 (50–92.86)	80.00 (53.33–100)	76.92 (61.22–100)	75.00 (61.90–91.33)	39.78
Clinical nomogram							
Training	0.70 (0.62–0.79)	67.48 (59.35–75.61)	68.75 (56.25–81.25)	66.67 (56.00–77.33)	56.90 (48.31–65.95)	76.92 (69.23–84.75)	156.9
Test	0.65 (0.49–0.8)	61.54 (48.08–75.00)	61.90 (42.86–80.95)	61.29 (45.16–77.42)	52.00 (37.50–66.67)	70.37 (57.14–84.40)	69.83
External	0.63 (0.43–0.83)	44.83 (24.14–65.52)	42.86 (14.29–71.43)	46.67 (20.00–73.33)	42.86 (20.75–62.50)	46.67 (26.98–65.79)	43.49

an AUC of 0.70 (95% CI: 0.62–0.79), 0.65 (95% CI: 0.49–0.80) and 0.63 (95% CI: 0.43–0.83) in the training, test and external test cohorts, respectively (Details are shown in Table 2).

We then incorporated the RS into the clinical prediction model using further multivariate logistic regression analysis (Supplementary Table S2), and this is presented as radiomics nomogram shown in Fig. 3a. There was significant difference of the nomogram-estimated probability between cachexic and non-cachexic patients in both training ($p < 0.001$), test ($p = 0.001$) and external test ($p = 0.031$) cohorts (Fig. 3b). Addition of the RS to the clinical model improved the prediction ability with AUCs of 0.78 (95% CI: 0.69–0.86, $p = 0.03$, Delong test), 0.76 (95% CI: 0.61–0.89, $p = 0.047$, Delong test) and 0.70 (95% CI: 0.52–0.89, $p = 0.61$) in the training, test and external test cohorts, respectively (Details are shown in Table 2). Further, the inclusion of RS yielded a total net reclassification improvement (NRI) of 0.91 (95% CI: 0.59–1.23, $p < 0.001$), 0.91 (95% CI: 0.43–1.39, $p < 0.001$) and 0.42 (95% CI:−001 to 0.86, $p = 0.05$) in the training, test and external test cohorts, respectively, which further showed significantly improved classification accuracy for cachexia prediction over clinical variables alone.

Qualitatively, calibration curves (Fig. 3c) indicate the agreement between the estimated probability and the actual cachexia rate based on the training ($p = 0.85$), test ($p = 0.85$) and external test ($p = 0.20$) cohorts, respectively. Decision curve analyses (Fig. 3d) show the performance of the RS, clinical model, and radiomics nomogram model in clinical application in both training and test cohorts. These show that the combined nomogram model has significant advantages compared to schema wherein either all or no patients are assumed to have cachexia. When comparing the three models, the radiomics nomogram model had the highest overall net clinical benefit across the threshold probabilities within the range of 0.30–0.60 in both cohorts.

Although addition of RS significantly improves predictive value of the clinical data (*vide supra*), the inverse was not true. There were no significant differences in predictive ability in both training ($p = 0.58$), and test ($p = 0.79$) and external test ($p = 0.62$) cohorts when comparing the RS alone with the combined nomogram. Even for the 57 patients without a history of cachexia, the combined nomogram achieved higher but also not significant AUC of 0.86 (95% CI: 0.74–0.97, $p < 0.001$), compared to the RS alone ($p = 0.071$, Delong test). Therefore, only RS alone was used as the final cachexia prediction biomarker and used for the following prognostic investigation.

Prognostic value of the radiomics signature in immunotherapy

The cachexia prediction RSs of the patients who experienced durable clinical benefit (DCB, PFS > 6 months) were significantly lower compared to those who did not in both the training (0.32 vs. 0.46, $p < 0.001$) and test (0.37 vs. 0.43, $p = 0.060$) cohorts. Similar results could be found in the external VA test patients (0.38 vs 0.47, $p = 0.048$). The AUCs of the RS to identify the DCB patients were 0.71 (95% CI: 0.61–0.80, $p < 0.001$), 0.66 (95% CI: 0.51–0.81, $p = 0.045$) and 0.70 (95% CI: 0.51–0.88, $p = 0.047$) in the training, test and external VA test cohorts, respectively.

For the training patients, the PFS and OS were significantly longer among patients with a RS below median value of 0.40 compared to patients with high (>0.40) RS (PFS: hazard ratio [HR]:1.73, 95% CI: 1.10–2.73, $p = 0.018$; OS: HR: 2.32, 95% CI:1.17–4.63, $p = 0.017$). Among patients with low RS, the median PFS was 11.00 months compared to 5.90 months or patients with high RS (PFS: $P = 0.016$, Fig. 4a). Median OS was not reached in the low RS group and was 19.77 months in the high RS group ($p = 0.014$, Fig. 4b). For the test patients, similar results could also be observed in training cohort with HR of 2.18 (95% CI: 1.09–4.38, $p = 0.028$) and 2.62 (95% CI: 1.05–6.56, $p = 0.040$) for PFS and OS estimation, respectively. Median PFS of the patients with low RS was significantly longer with 17.00 months versus 4.17 months ($p = 0.024$, Fig. 4c), and the median OS was also not reached in the low RS group and was 19.77 months in the high RS group ($p = 0.014$, Fig. 4d). Through log-rank test, there was no significant difference between RS and real occurrence of cachexia. The external VA test patients further validate the prognostic value of RS with HRs of 3.84 (95% CI: 1.56–9.43, $p = 0.049$) and 2.63 (95% CI: 1.02–6.83, $p = 0.046$) for PFS (4.77 vs 12.97 months, $p = 0.002$, Fig. 4e) and OS (8.37 vs 22.17 months, $p = 0.039$, Fig. 4f), respectively.

Complementary prognostic value of the radiomics signature on potentially sensitive patients

Of 106 patients with known PD-L1 status, 63 were positive (TPS ≥ 1%) and 43 were negative for PD-L1 expression. In the PD-L1 positive cohort, the median PFS and OS were significantly longer in the low RS group compared to the high RS group. The median PFS was not reached in the low RS group versus 4.87 months in the high RS group (Log-rank $p < 0.01$, Fig. 4g). The median OS was not reached in the low RS group versus 13.03 months in the high RS group ($p = 0.035$, Fig. 4i). In contrast, in PD-L1-negative patients, there were no significant differences between low and high RS scores in their PFS ($p = 0.30$, Fig. 4h) or OS ($p = 0.19$, Fig. 4j). However, it is worth noting that the K–M curve for PFS of PD-L1-negative patients (Fig. 4i) shows significant differences between low and high RS scores for the first 9 months, but then evened out and became insignificant. This is notable because a PFS > 6 months is considered a DCB and thus, in this case, the RS was able to distinguish among PD-L1 patients with and without a

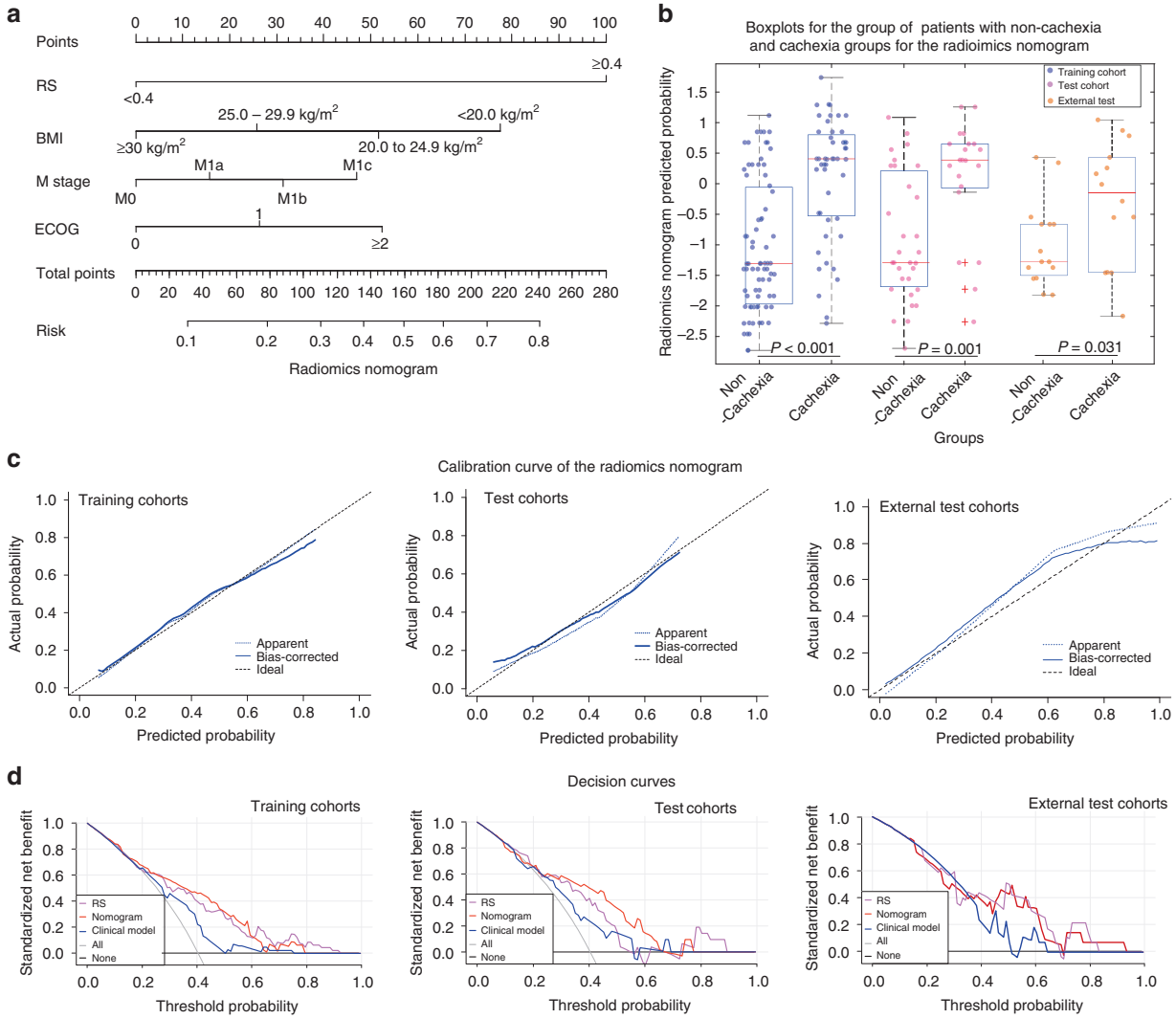

Fig. 3 Radiomics Nomograms. a The nomogram constructed with RS and clinical variables to estimate the risk of cachexia. **b** The box plot of nomogram predicted cachexia probability of individual. In the boxplots, the central line represents the median, the bounds of box the first and third quartiles, and the whiskers are the interquartile range. The blue points represent the training cohort, the magenta points represent the test cohort, and the orange points represent the external test cohort. *P*-value shows two-sided Wilcoxon signed-rank test. **c** The assessment of the model calibration in the training, test and external test cohorts. **d** The decision curves of RS, radiomics nomogram and clinical model in the training and test cohorts.

DCB ($p < 0.05$, Fig. 4k, l). These results further indicated the complementary prognostic value of RS on the ICI treatment among PD-L1-positive patients, that is, those that are potentially sensitive to ICI. The multivariable Cox analysis identified RS and PD-L1 as independent prognostic predictors of PFS (RS: hazard ratio (HR) = 2.25, 95% confidence interval (CI): 1.39–3.63; $p = 0.001$; PD-L1: HR: 0.51, 95% CI: 0.32–0.81, $p = 0.004$) and OS (RS: HR = 2.18, 95% CI: 1.12–4.23; $p = 0.021$; PD-L1: HR: 0.48, 95% CI: 0.26–0.90, $p = 0.022$).

Radiomic quality score

Radiomics is a rapidly maturing field in machine learning. To rigorously assess the quality of study design, a 36-point "Radiomics Quality Score" (RQS) metric that evaluates 16 different key components was used. The full list of criteria and the corresponding score are described in Supplementary Table S4, which shows that the current study had an RQS of 17. According to a recent meta-analysis[40] that analysed 77 radiomics publications and documented that the mean ± S.D. RQS across all studies was 9.4 ± 5.6, the current study is in the upper 20 percentage of radiomics study designs. Finally, a TRIPOD Checklist following reporting guidelines for prediction model development and validation has also been provided in Supplementary Table S5, which further validated the integrity of the work.

DISCUSSION

In this study we conducted a rigorous radiomics analyses to develop a pre-treatment radiomics model to predict development of cachexia after the initiation of ICI. Cancer cachexia is a multifactorial wasting syndrome defined by involuntary progressive weight loss[41] that may be induced by cancer or by cancer therapy.[1] Regardless of the cause, both cancer-induced and therapy-induced cachexia promote resistance to ICI, so we did not attempt to distinguish the underlying cause in this study. Overall, we found that BMI, distant metastasis, ECOG and the radiomics signature (RS) of diagnostic PET/CT images, were significant and independent predictors of cachexia in patients with advanced stage NSCLC treated with immunotherapy. Importantly, these data can be routinely captured during patient workup as standard-of-

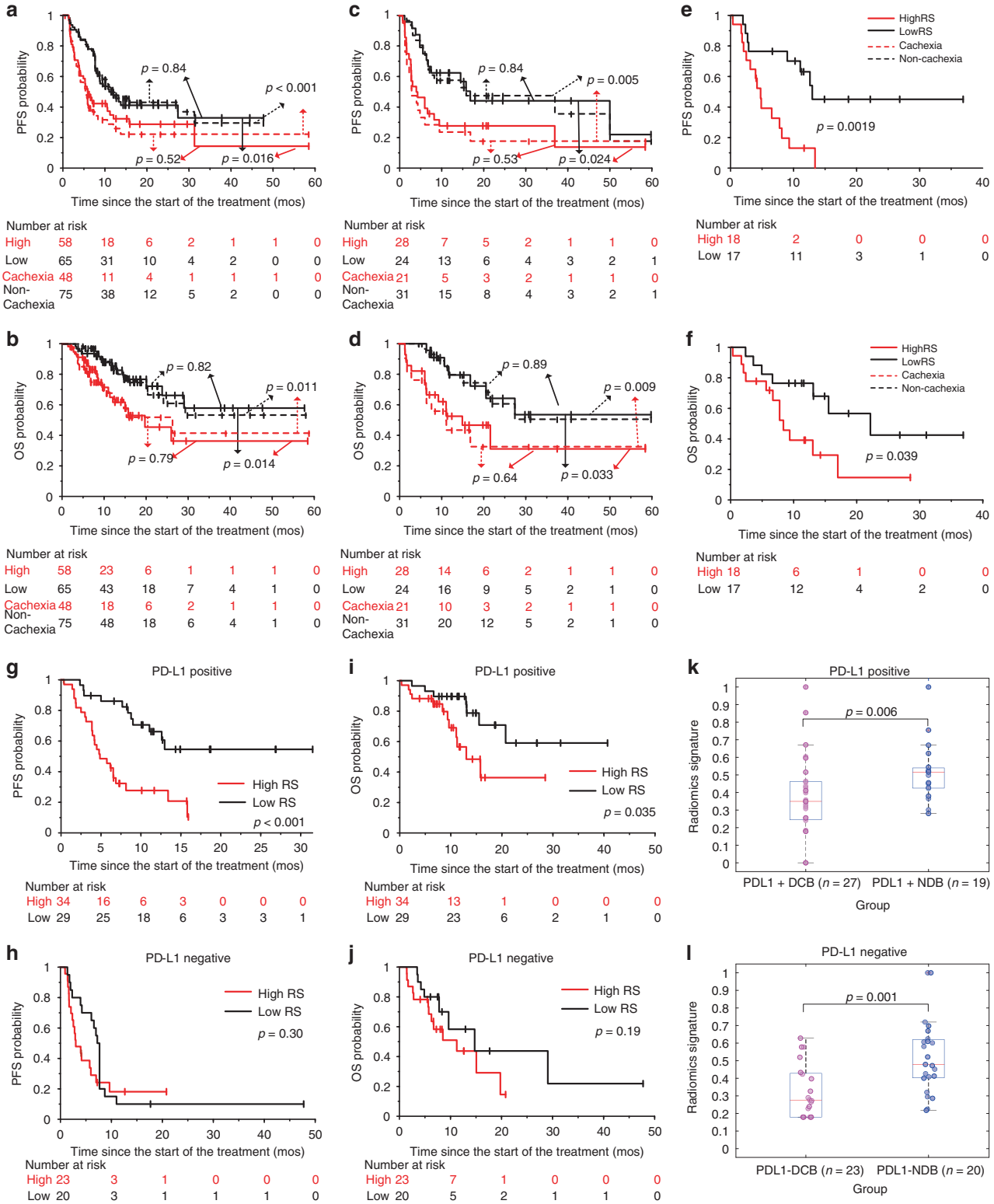

Fig. 4 Prognostic ability of RS in various cohorts. a, b The Kaplan–Meier survival curves of PFS and OS relative to the RS, and the real cachexia status in the training cohort, respectively. **c, d** The Kaplan–Meier survival curves of PFS and OS relative to the RS, and the real cachexia status in the test cohort, respectively. **e, f** The Kaplan–Meier survival curves of PFS and OS relative to the RS in the external VA cohort, respectively. **g, h** The Kaplan–Meier survival curves of PFS relative to the RS in the sub cohort with PD-L1 positive status, and PD-L1 negative status, respectively. **i, j** The Kaplan–Meier survival curves of OS relative to the RS in the sub cohort with PD-L1 positive status, and PD-L1 negative status, respectively. **k, l** The comparison of the radiomics signatures (RSs) of patients with DCB and NDB (non-durable benefit, PFS < 6 months) in the sub cohort with PD-L1-positive status, and PD-L1-negative status, respectively. Comparisons of the above PFS and OS curves were performed with a two-sided log-rank test. The comparison of RS between two groups was performed with Wilcoxon sign rank test.

care. The radiomics signature developed in this work further showed significant prognostic value, especially among those potentially immunotherapy sensitive patients with PD-L1-positive status. Therefore, this approach has the potential to be used to optimise patient management and treatment planning with early interventions prior to the start of immunotherapy pending on a further multi-institution prospective validation with larger cohorts.

Many previous studies have attempted to identify predictive biomarkers of cachexia. Given that cachexia is defined primarily by unintended weight loss, several studies have investigated and shown the cachexia-indicative value of initial weight loss.[14–16,42] Additionally, BMI,[14] ECOG PS, biochemistry (high C-reactive protein, leukocytes, hypoalbuminemia or anaemia),[16] cancer type and COPD[42] have also been used to construct cachexia prediction models. Further, CT-based SMI was shown to be predictive of cachexia and survival of patients with cancer.[32] However, none of these variables characterised the metabolic changes, characteristic of cancer-associated cachexia. Recently, Interleukin (IL)-8 was demonstrated to induce myotube atrophy, which indicated the potential of IL-8 to define the cachectic state in NSCLC patients.[43] Additionally, de Jong et al. found longitudinal differences in CT-based radiomic features that were related to cachexia with an AUC of 0.68.[44] To the best of our knowledge, this study is the first to predict development of cachexia directly using baseline PET/CT images before the start of the immunotherapy, with AUCs of the combined model approaching 0.76 in independent testing.

Determination of the regions of interest (ROI) to perform analysis is challenging. For example, since sarcopenia is a hallmark of cachexia, it could be that the skeletal muscles are the most strongly affected, but it is also likely that the triggering signals arise from the tumour itself. Skeletal muscle CT radiomic features were investigated by de Jong et al, but the baseline features could not predict future muscle loss in NSCLC patients, and follow-up PET/CT images were not always available.[44] Additionally, mediators released from cancer cells and cells within the tumour microenvironment have been considered to be associated with cachexia in lung cancers.[43] Given our assumption that the primary nodule provides pertinent genetic and microenvironmental information,[45,46] our radiomic analysis was confined to the primary nodule.

When investigating the informative components of RS formula, we found the longest diameter of the tumour (PET_{LD}) was negatively correlated with risk of cachexia, suggesting that tumours with smaller diameter may have higher risk of cachexia. This is consistent with previous studies saying patients with small tumour volumes are often diagnosed with cachexia, whereas this syndrome may never develop in patients with large tumour burdens.[47,48] In term of the negative correlation of CT_{max} and positive correlation of $PETlow_{LZLGE}$ with the risk of cachexia, tumours with low intensity had a higher probability of cachexia, since low intensity lesions often include oedema and necrosis, which is capable of inducing cachexia.[49] The remaining informative features are texture features (CT_{ZSN}, CT_{energy}), suggesting that heterogeneity increases the risk of cachexia, which is consistent with the observation that more heterogeneous tumours are usually more aggressive.[50]

When investigating the relationship between clinical characteristics and cachexia, BMI, ECOG PS, and distant metastasis were highly correlated with cachexia, which are consistent with most other studies. For the investigation of initial weight loss, though the weight loss of the past 6 months and 2 months were also significant factors with OR of 0.85 (95% CI: 0.71–1.01, $p = 0.056$) and 0.78 (95% CI: 0.61–1.00, $p = 0.049$) in the patients who have history weight loss record before the start of the immunotherapy in our study, this factor was not included in the multivariable analysis in our study due to its unavailability for most of the patients.

For the comparison between RS and SMI,[32] SMI was not significantly predictive in the whole cohort (training: $p = 0.28$, test: $p = 0.24$). Although SMI was found predictive in further stratified analysis performed on the patients without a history of cachexia, its predictive ability was similar to RS ($p = 0.57$, Delong test). Notably, RS was significantly predictive regardless the historical cachexia status, indicating that the RS may have more clinical significance.

Through the prognostic analysis, we observed that cachexia is significantly correlated with a short PFS and OS in response to ICI, which is consistent with literature.[19] Compared to the presence of cachexia, our predicted RS based on the baseline PET/CT images obtain the similar separation of the Kaplan–Meier PFS and OS survival curves prior to the start of weight loss associated with ICI treatment. Therefore, the cachexia prediction RS could also be regarded a prognostic biomarker for immunotherapy and may help to identify patients who are more likely to achieve a durable clinical benefit. According to the stratified analysis based on PD-L1 status and RS, within the PD-L1 positive group that is more sensitive for immunotherapy, patients with low RS, i.e. low risk of cachexia had significantly longer OS and PFS compared to high RS patients, while there was no difference within the PD-L1-negative group. One potential explanation of this may be the down-regulation of PD-1 or PD-L1 receptors due to the cachexia,[51,52] which may indicate that cachexia induced PD-L1 downregulation may be one of the reasons for the resistance of immunotherapy during the treatment. It's also notable that, within the PD-L1 negative group, significant differences in PFS in the early 9 months (especially for the first 6 months, DCB) were found, but these eventually evened out and became insignificant. The possible reason could be cachexia is significantly correlated with shorter PFS before the emergence of resistance of ICI, as median duration of response for PD-L1 negative advanced NSCLC patients treated with ICI is 8.5 months.[53] Beyond this median response time, all patients tend to have poor prognosis regardless of the cachexia status.

The present study does possess some limitations. First, the sample size of patients with recorded weight loss was small relative to the entire cohort, which means the predictive value of initial weight loss for the whole cohort could not be incorporated into the prediction model. However, initial weight loss was unavailable for many patients, especially for those who received first-line immunotherapy after the diagnosis, which means the clinical use of a model with initial weight loss may be limited. Second, the patient cohorts were heterogeneous in terms of PET/CT image acquisition. However, this also be viewed as a strength of the current approach, and the prognostic value in the external test cohort showed that the developed radiomics signature is robust and transportable. Third, follow-up PET/CT images were not available for most of the patients and hence, longitudinal differences in skeletal muscle and tumour radiomics features could not be analysed and compared. Lastly, our study was performed on PET/CT images, wherein the CT is not contrast-enhanced and lacks much of the peritumoural info. Hence, we focused on the primary tumour in this study without extracting the features from peritumoural regions, even though these may reflect the tumour immune microenvironment.[54] A parallel study using contrast-enhanced computed tomography (CE-CT) images for the prediction will be performed with the addition of peritumoural image features. Despite these deficiencies, the predictive value of the RS and/or combined nomogram was high and clinically actionable. If patients have a high probability of developing cachexia and hence poor outcome, it is recommended that their nutritional status be rigorously monitored throughout the initial phase of therapy. Besides lung cancer, oesophageal cancer, head and neck cancer, gastric cancer and pancreatic cancer are also major cachexia-causing cancers. Among these, oesophageal as well as head and neck cancer are often monitored with FDG PET/CT,

while contrast-enhanced computed tomography (CE-CT) or MRI are more commonly used in the staging of gastric and pancreatic cancer. Thus, it is possible that the current trained model could be directly applied to oesophageal or head and neck cancer, but to extend these approaches to gastric and pancreatic cancer would require construction of novel models with the analysis of both tumour and host factors to identify cachexia.

CONCLUSION

In conclusion, a novel radiomics signature from pre-treatment PET/CT images has been identified and may serve as a potential predictive biomarker to identify both patients who at risk of developing cachexia after the start of the immunotherapy, and patients most likely to benefit from immunotherapy especially from those potentially immunotherapy sensitive patients with PD-L1 positive status. Due to the advantage of being based on routinely acquired patient information and its non-invasive characteristic, this signature could be used for optimising the treatment plan pending on multi-institution, larger and prospective trials.

ACKNOWLEDGEMENTS

We sincerely thank orthopaedist (ret.) Yi Wang (wangyi999888@163.com) for the skeletal muscle identification, and Jin Qi from H. Lee Moffitt Cancer Center & Research Institute for her kind help in refining the tumour segmentation.

AUTHOR CONTRIBUTIONS

The authors meet criteria for authorship as recommended by the International Committee of Medical Journal Editors. W.M., C.J.W., K.L.G., M.B.S. and R.J.G. contributed to the conception and design of the work; W.M. designed the model and the computational framework and analysed the data; E.K. and W.M. collected the image and clinical data; M.B.S. and R.J.G. supervised the study; M.B.S. and R.J.G. revised the work critical for important intellectual content. All authors contributed to the production of the final manuscript.

ADDITIONAL INFORMATION

Ethical approval and consent to participate All procedures performed in studies involving human participants were in accordance with the ethical standards of the Institutional Review Board at the University of South Florida (USF) and with the 1964 Helsinki declaration and its later amendments or comparable ethical standards. The requirement for informed consent was waived because of the retrospective nature of the study.

Data availability The PET/CT imaging data and clinical information are not publicly available for patient privacy purposes but are available from the corresponding authors upon reasonable request (R.J.G. and M.B.S.). The remaining data are available within the Article and Supplementary Information.

Competing interests R.J.G. declared a potential conflict with HealthMyne, Inc [Investor, Board of Advisors]. Contents of this research do not represent the views of the Department of Veterans Affairs or the United States Government. The remaining authors declare no competing interests.

Funding information This study was funded by U.S. Public Health Service research grant U01 CA143062 and R01 CA190105 (awarded to R.J.G.).

The online version contains supplementary material available at https://doi.org/10.1038/s41416-021-01375-0.

REFERENCES

1. Fearon, K., Arends, J. & Baracos, V. Understanding the mechanisms and treatment options in cancer cachexia. *Nat. Rev. Clin. Oncol.* **10**, 90–99 (2013).
2. Vagnildhaug, O. M., Balstad, T. R., Almberg, S. S., Brunelli, C., Knudsen, A. K., Kaasa, S. et al. A cross-sectional study examining the prevalence of cachexia and areas of unmet need in patients with cancer. *Support Care Cancer* **26**, 1871–1880 (2018).
3. Tisdale, M. J. Cachexia in cancer patients. *Nat. Rev. Cancer* **2**, 862–871 (2002).
4. Fearon, K., Strasser, F., Anker, S. D., Bosaeus, I., Bruera, E., Fainsinger, R. L. et al. Definition and classification of cancer cachexia: an international consensus. *Lancet Oncol.* **12**, 489–495 (2011).
5. Muscaritoli, M., Bossola, M., Aversa, Z., Bellantone, R. & Fanelli, F. R. Prevention and treatment of cancer cachexia: new insights into an old problem. *Eur. J. Cancer* **42**, 31–41 (2006).
6. Baracos, V. E., Martin, L., Korc, M., Guttridge, D. C. & Fearon, K. C. Cancer-associated cachexia. *Nat. Rev. Dis. Prim.* **4**, 1–18 (2018).
7. Young, R. P., Hopkins, R. J., Christmas, T., Black, P. N., Metcalf, P. & Gamble, G. D. COPD prevalence is increased in lung cancer, independent of age, sex and smoking history. *Eur. Respir. J.* **34**, 380–386 (2009).
8. Wagner, P. Possible mechanisms underlying the development of cachexia in COPD. *Eur. Respir. J.* **31**, 492–501 (2008).
9. Jo, H., Horinouchi, H., Yagishita, S., Shinno, Y., Okuma, Y., Yoshida, T. et al. Impact of cachexia in advanced NSCLC patients treated with PD-1 inhibitor. *J. Clin. Oncol.* **38**(5_suppl), 44 (2020).
10. Reck, M., Rodríguez-Abreu, D., Robinson, A. G., Hui, R., Csőszi, T., Fülöp, A. et al. Pembrolizumab versus chemotherapy for PD-L1–positive non–small-cell lung cancer. *N. Engl. J. Med.* **375**, 1823–1833 (2016).
11. Brocco, D., Di Marino, P. & Grassandonia, A. From cachexia to obesity: the role of host metabolism in cancer immunotherapy. *Curr. Opin. Support Palliat. Care* **13**, 305–310 (2019).
12. Turner, D. C., Kondic, A. G., Anderson, K. M., Robinson, A. G., Garon, E. B., Riess, J. W. et al. Pembrolizumab exposure–response assessments challenged by association of cancer cachexia and catabolic clearance. *Clin. Cancer Res.* **24**, 5841–5849 (2018).
13. Laird, B. & Fallon, M. Treating cancer cachexia; an evolving landscape. *Ann. Oncol.* **28**, 2055–2056 (2017).
14. Blum, D., Stene, G. B., Solheim, T. S., Fayers, P., Hjermstad, M. J., Baracos, V. E. et al. Validation of the consensus-definition for cancer cachexia and evaluation of a classification model—a study based on data from an international multicentre project (EPCRC-CSA). *Ann. Oncol.* **25**, 1635–1642 (2014).
15. van der Meij, B. S., Schoonbeek, C. P., Smit, E. F., Muscaritoli, M., van Leeuwen, P. A. & Langius, J. A. Pre-cachexia and cachexia at diagnosis of stage III non-small-cell lung carcinoma: an exploratory study comparing two consensus-based frameworks. *Br. J. Nutr.* **109**, 2231–2239 (2013).
16. Vigano, A. A. L., Morais, J. A., Ciutto, L., Rosenthall, L., di Tomasso, J., Khan, S. et al. Use of routinely available clinical, nutritional, and functional criteria to classify cachexia in advanced cancer patients. *Clin. Nutr.* **36**, 1378–1390 (2017).
17. Schmidt, S. F., Rohm, M., Herzig, S. & Diaz, M. B. Cancer cachexia: more than skeletal muscle wasting. *Trends Cancer* **4**, 849–860 (2018).
18. Tisdale, M. J. Are tumoral factors responsible for host tissue wasting in cancer cachexia? *Future Oncol.* **6**, 503–513 (2010).
19. Devlin, M. J., Cloutier, A. M., Thomas, N. A., Panus, D. A., Lotinun, S., Pinz, I. et al. Caloric restriction leads to high marrow adiposity and low bone mass in growing mice. *J. Bone Min. Res.* **25**, 2078–2088 (2010).
20. Barreto, R., Mandili, G., Witzmann, F. A., Novelli, F., Zimmers, T. A. & Bonetto, A. Cancer and chemotherapy contribute to muscle loss by activating common signaling pathways. *Front. Physiol.* **7**, 472 (2016).
21. Hiensch, A. E., Bolam, K. A., Mijwel, S., Jeneson, J. A., Huitema, A. D., Kranenburg, O. et al. Doxorubicin-induced skeletal muscle atrophy: elucidating the underlying molecular pathways. *Acta Physiol.* **229**, e13400 (2020).
22. Damrauer, J. S., Stadler, M. E., Acharyya, S., Baldwin, A. S., Couch, M. E. & Guttridge, D. C. Chemotherapy-induced muscle wasting: association with NF-κB and cancer cachexia. *Eur. J. Transl. Myol.* **28**, 7590 (2018).
23. Braun, T. P., Szumowski, M., Levasseur, P. R., Grossberg, A. J., Zhu, X., Agarwal, A. et al. Muscle atrophy in response to cytotoxic chemotherapy is dependent on intact glucocorticoid signaling in skeletal muscle. *PLoS ONE* **9**, e106489 (2014).
24. Courtois, A., Nusgens, B. V., Hustinx, R., Namur, G., Gomez, P., Somja, J. et al. 18F-FDG uptake assessed by PET/CT in abdominal aortic aneurysms is associated with cellular and molecular alterations prefacing wall deterioration and rupture. *J. Nucl. Med.* **54**, 1740–1747 (2013).
25. Shozushima, M., Tsutsumi, R., Terasaki, K., Sato, S., Nakamura, R. & Sakamaki, K. Augmentation effects of lymphocyte activation by antigen-presenting macrophages on FDG uptake. *Ann. Nucl. Med.* **17**, 555–560 (2003).
26. Aerts, H. J., Velazquez, E. R., Leijenaar, R. T., Parmar, C., Grossmann, P., Carvalho, S. et al. Decoding tumour phenotype by noninvasive imaging using a quantitative radiomics approach. *Nat. Commun.* **5**, 1–9 (2014).

27. Mu, W., Jiang, L., Zhang, J., Shi, Y., Gray, J. E., Tunali, I. et al. Non-invasive decision support for NSCLC treatment using PET/CT radiomics. *Nat. Commun.* **11**, 5228 (2020).
28. Mu, W., Tunali, I., Qi, J., Schabath, M. B. & Gillies, R. J. Radiomics of 18F fluorodeoxyglucose PET/CT images predicts severe immune-related adverse events in patients with NSCLC. *Radio. Artif. Intell.* **2**, e190063 (2020).
29. Mu, W., Tunali, I., Gray, J. E., Qi, J., Schabath, M. B. & Gillies, R. J. Radiomics of 18 F-FDG PET/CT images predicts clinical benefit of advanced NSCLC patients to checkpoint blockade immunotherapy. *Eur. J. Nucl. Med. Mol. Imaging* **47**, 1168–1182 (2020).
30. Zhang, J., Zhao, X., Zhao, Y., Zhang, J., Zhang, Z., Wang, J. et al. Value of pre-therapy 18 F-FDG PET/CT radiomics in predicting EGFR mutation status in patients with non-small cell lung cancer. *Eur. J. Nucl. Med. Mol. Imaging* **47**, 1137–1146 (2020).
31. Jiang, M., Sun, D., Guo, Y., Guo, Y., Xiao, J., Wang, L. et al. Assessing PD-L1 expression level by radiomic features from PET/CT in nonsmall cell lung cancer patients: an initial result. *Acad. Radio.* **27**, 171–179 (2020).
32. Martin, L., Birdsell, L., MacDonald, N., Reiman, T., Clandinin, M. T., McCargar, L. J. et al. Cancer cachexia in the age of obesity: skeletal muscle depletion is a powerful prognostic factor, independent of body mass index. *J. Clin. Oncol.* **31**, 1539–1547 (2013).
33. Mu, W., Chen, Z., Shen, W., Yang, F., Liang, Y., Dai, R. et al. A segmentation algorithm for quantitative analysis of heterogeneous tumors of the cervix with 18 F-FDG PET/CT. *IEEE Trans. Biomed. Eng.* **62**, 2465–2479 (2015).
34. Otsu, N. A threshold selection method from gray-level histograms. *IEEE Trans. Syst. Man Cyber. Syst.* **9**, 62–66 (1979).
35. Zwanenburg, A., Vallières, M., Abdalah, M. A., Aerts, H. J., Andrearczyk, V., Apte, A. et al. The image biomarker standardization initiative: standardized quantitative radiomics for high-throughput image-based phenotyping. *Radiol* **295**, 328–338 (2020).
36. Friedman, J., Hastie, T. & Tibshirani, R. Regularization paths for generalized linear models via coordinate descent. *J. Stat. Softw.* **33**, 1 (2010).
37. Lambin, P., Leijenaar, R. T., Deist, T. M., Peerlings, J., De Jong, E. E., Van Timmeren, J. et al. Radiomics: the bridge between medical imaging and personalized medicine. *Nat. Rev. Clin. Oncol.* **14**, 749–762 (2017).
38. Huang, Y.-q, Liang, C.-h, He, L., Tian, J., Liang, C.-s, Chen, X. et al. Development and validation of a radiomics nomogram for preoperative prediction of lymph node metastasis in colorectal cancer. *J. Clin. Oncol.* **34**, 2157–2164 (2016).
39. DeLong, E., DeLong, D. & Clarke-Pearson, D. Comparing the areas under two or more correlated receiver operating characteristic curves: a nonparametric approach. *Biometrics* **44**, 837–845 (1988).
40. Park, J. E., Kim, D., Kim, H. S., Park, S. Y., Kim, J. Y., Cho, S. J. et al. Quality of science and reporting of radiomics in oncologic studies: room for improvement according to radiomics quality score and TRIPOD statement. *Eur. Radiol.* **30**, 523–536 (2020).
41. Vanhoutte, G., van de Wiel, M., Wouters, K., Sels, M., Bartolomeeussen, L., De Keersmaecker, S. et al. Cachexia in cancer: what is in the definition? *BMJ Open Gastroenterol.* **3**, e000097 (2016).
42. Vagnildhaug, O. M., Brunelli, C., Hjermstad, M. J., Strasser, F., Baracos, V., Wilcock, A. et al. A prospective study examining cachexia predictors in patients with incurable cancer. *BMC Palliat. Care* **18**, 1–10 (2019).
43. Santiloni Cury, S., De Moraes, D., Paccielli Freire, P., De Oliveira, G., Venâncio Pereira Marques, D., Javier Fernandez, G. et al. Tumor transcriptome reveals high expression of IL-8 in non-small cell lung cancer patients with low pectoralis muscle area and reduced survival. *Cancers* **11**, 1251 (2019).
44. de Jong, E., Sanders, K., Deist, T., van Elmpt, W., Jochems, A., van Timmeren, J. et al. Can radiomics help to predict skeletal muscle response to chemotherapy in stage IV non-small cell lung cancer? *Eur. J. Cancer* **120**, 107–113 (2019).
45. Curtis, S. J., Sinkevicius, K. W., Li, D., Lau, A. N., Roach, R. R., Zamponi, R. et al. Primary tumor genotype is an important determinant in identification of lung cancer propagating cells. *Cell Stem Cell* **7**, 127–133 (2010).
46. Laughney, A. M., Hu, J., Campbell, N. R., Bakhoum, S. F., Setty, M., Lavallée, V. P. et al. Regenerative lineages and immune-mediated pruning in lung cancer metastasis. *Nat. Med.* **26**, 259–269 (2020).
47. Couch, M., Lai, V., Cannon, T., Guttridge, D., Zanation, A., George, J. et al. Cancer cachexia syndrome in head and neck cancer patients: Part I. Diagnosis, impact on quality of life and survival, and treatment. *Head. Neck* **29**, 401–411 (2007).
48. Tisdale, M. J. Molecular pathways leading to cancer cachexia. *Physiol* **20**, 340–348 (2005).
49. Stephens, K. E., Ishizaka, A., Larrick, J. W. & Raffin, T. A. Tumor necrosis factor causes increased pulmonary permeability and edema. *Am. Rev. Respir. Dis.* **137**, 1364–1370 (1988).
50. Bashir, U., Siddique, M. M., Mclean, E., Goh, V. & Cook, G. J. Imaging heterogeneity in lung cancer: techniques, applications, and challenges. *Am. J. Roentgenol.* **207**, 534–543 (2016).
51. Khaddour, K., Gomez-Perez, S. L., Jain, N., Patel, J. D. & Boumber, Y. Obesity, sarcopenia, and outcomes in non-small cell lung cancer patients treated with immune checkpoint inhibitors and tyrosine kinase inhibitors. *Front. Oncol.* **10**, 576314 (2020).
52. Cheng, B., Ren, Y., Cao, H. & Chen, J. Discovery of novel resorcinol diphenyl ether-based PROTAC-like molecules as dual inhibitors and degraders of PD-L1. *Eur. J. Med. Chem.* **199**, 112377 (2020).
53. Borghaei, H., Langer, C. J., Paz-Ares, L., Rodríguez-Abreu, D., Halmos, B., Garassino, M. C. et al. Pembrolizumab plus chemotherapy versus chemotherapy alone in patients with advanced non–small cell lung cancer without tumor PD-L1 expression: a pooled analysis of 3 randomized controlled trials. *Cancer* **126**, 4867–4877 (2020).
54. Jiang, Y., Wang, H., Wu, J., Chen, C., Yuan, Q., Huang, W. et al. Noninvasive imaging evaluation of tumor immune microenvironment to predict outcomes in gastric cancer. *Ann. Oncol.* **31**, 760–768 (2020).